

Structural connectivity modifications in the brain of selected patients with tumour after its removal by surgery (a case study)

Elaheh Sayari¹, Evandro G. Seifert¹, Fátima E. Cruziniani², Enrique C. Gabrick¹, Kelly C. Iarosz^{1,3,4}, José D. Szezech Jr.^{1,5}, Murilo S. Baptista⁶, Iberê L. Caldas⁴, Antonio M. Batista^{1,4,5}

¹*Graduate Program in Science, State University of Ponta Grossa, 84030-900, Ponta Grossa, PR, Brazil.*

²*Department of Physics, State University of Ponta Grossa, 84030-900, Ponta Grossa, PR, Brazil.*

³*University Center UNIFATEB, 84266-010, Telêmaco Borba, PR, Brazil.*

⁴*Physics Institute, University of São Paulo, 05508-090, São Paulo, SP, Brazil.*

⁵*Department of Mathematics and Statistics, State University of Ponta Grossa, 84030-900, Ponta Grossa, PR, Brazil.*

⁶*Institute for Complex Systems and Mathematical Biology, University of Aberdeen, AB24 3UE, Aberdeen, Scotland, United Kingdom.*

Abstract

The brain is a complex organ that plays an important role in the control of most functions of the body, such as awareness, thoughts, sensations, movements, speech, and memory. A tumour formed in the brain can affect its ability to accurately and properly perform such functions. In this work, we use two brains with malignant tumours of different sizes before and after surgery. To identify the brain structural topology, we analyse different networks with various configurations and use diagnostic tools to match the network topologies generated by simulations with those obtained from the data. Our results show that the Newman-Watts small-world network best reproduces the topology from the patients with small and large tumours before surgery. Considering two analysed brains, our outcomes suggest that surgery

*Corresponding author: sayarielaheh@gmail.com

can alter the brain topology from small-world to extended Barabási-Albert scale-free.

Keywords: Complex system, Brain tumour, Structural connectivity matrix, Graph theory

1. Introduction

A brain tumour is a mass or growth of abnormal cells that may be non-cancerous (benign) or cancerous (malignant) [1]. The benign brain tumours grow slowly and do not spread to the whole brain or central nervous system, while the malignant ones grow and spread rapidly and can cause some serious problems for a patient [2]. The malignant tumours can be separated into several groups with variant grades, such as diffuse astrocytic and oligodendroglial tumours, glioblastomas, other gliomas, ependymal tumours, melanocytic tumours, lymphomas, germ cell tumours, moreover extrinsic tumours such as meningiomas. They are described by their malignancy according to the World Health Organisation (WHO) grading system. With a ranking that the grade I tumours are least malignant compared to grade III meningioma or IV glioma tumours that are most malignant [3].

Magnetic resonance imaging (MRI) [4] and functional magnetic resonance imaging (fMRI) [5] provide the data from which the structural connection matrix and the functional connectivity matrix, respectively, can be obtained. These kinds of data have been used to analyse the neural bases of the human cognition and neurological disorders, such as Alzheimer's disease, brain tumours, and autism [6, 7]. The structural connectivity between two regions in the brain indicates the presence of white matter tracts that physically interconnect the cerebral areas, while functional connectivity describes the statistical relationships between the brain signals time series of blood oxygenation level-dependent (BOLD) over time [8]. In 1873, Golgi [9] made the glimpses of the complex branching of nerve cells using blocks of brain tissue soaked in silver-nitrate solution. It was one of the first experimental measurements of the brain's structural connectivity. Afterward, Cajal came to the understanding that neurons do not exist in solitude [1], forming complex networks of physical links. When the electron microscope in the 1930s was invented, it provided measurements of the physical links between neurons in more details [1]. Computerised axial tomography (CAT) introduced in the 1970s was considered as the most accurate anatomical imaging of the

human brain [1]. Thereafter, diffusion tensor imaging (DTI) as a remarkable example of magnetic resonance imaging (MRI) was developed [1]. These neuroimaging methods, CAT and MRI, capture cross-sectional images of the brain, while DTI reconstructs the large-scale neural pathways that link separate brain areas and tracks the diffusion of water molecules through white matter tracts [1].

Over the past several decades, there has been much investigation using MRI by scientists who study the physiology of human brain networks to map the human structural connectome in a wide variety of applications. According to Hilgetag et al. [1], the structural connectivity matrices of the cat and macaque show a complex structure, while, in humans, the structural connection matrix intercedes several complex cognitive functions [1].

To understand brain connectome or connectivity architecture in terms of the structural organisation, the graph theory-based method plays an important role in analysing connectivity patterns in human brain network [1]. A graph, in discrete systems, is a mathematical representation of a network, namely a representation of data in an organised manner, describing the relationship among lines (edges) and points (vertices). The human connectome has attracted the attention of many researchers in neuroscience, mainly in studies about network science and graph theory [1, 1], connectome studies in neuroscience have involved several different modalities [2]. These approaches have contributed to tackling a large number of practical problems in other fields, such as transportation systems [2], social networks [2], big data environments [2], and biological neural networks [2, 2]. In 1736, Euler [2] solved the Königsberg bridge problem considered to be the first application of graph analysis. Since 2009, after launching the Human Connectome Project, the application of graph theory for analysing the connectivity patterns of an individual brain has attracted the attention of many researchers [2]. In recent years, several studies about the relationship between the graph (or structure) and the behaviour (or function) of dynamical networks have increased [2, 2]. Graph theory provides concepts and their quantities to describe the brain structural network topology using various metrics, such as integration, segregation, centrality and density [2].

Watts and Strogatz [2] reported that a wide variety of social, biological, and geoscience-based networks have a remarkable structure, called small-world architecture. The small-world network has a combination of short path length comparable to a random network and of high clustering as compared with a regular network. In 2017, Liao et al. [3] showed that the human brain

network has a small-world architecture. Indeed, the metabolic and wiring costs of links between anatomically distant brain areas are greater than those of neighbouring brain areas [3]. From a theoretical point of view, to reduce the total metabolic cost, brain regions interact more with their neighbouring regions, while at the same time require a small number of remote connections to speed up data transfer [3].

Some studies focused on brain development and cognition [3, 3], as well as mental and neurological disorders [3, 3]. The brain adapts (or changes) also as a result of other disorders, and graph-theoretical approaches are very helping us to draw a comprehensive picture of how that happens. Many studies investigated neurological disorders, such as epilepsy [3], Alzheimer’s disease (AD) [3], autism spectrum disorder (ASD) [3], multiple sclerosis (MS) [4], and attention-deficit/hyperactivity disorder (AD HD) [4], as well as mental disorders, such as Parkinson’s disease [4], major depression [4], insomnia [4], borderline personality disorder (BPD) [4], schizophrenia [4], and obsessive compulsive disorder (OCD) [4] using graph theory. Yu et al. [4] has reported comparable structural network topology in brain tumour patients, with meningioma and glioma. They showed the increase of the connection density and the local efficiency, in the tumour group. The enhanced density in the tumour patients after surgery suggests that surgery may induce re-organisation in the structural network topology. Therefore, surgery causes significantly topological alterations in the patients with small and large tumour. Aerts et al. [4] assessed the structural network topology related to healthy control participants, meningioma and glioma patients with various graph theory metrics, such as global efficiency and modularity, using the Brain Connectivity Toolbox. They showed that differences in global efficiency and modularity in glioma patients compared to healthy controls and meningioma patients were not significant. Furthermore, in [3] it was shown that after the patients considered in [4] have undergone surgery, no significant changes occur in the graph metrics considered in [4] before the surgery.

In this work, our main purpose is to analyse the brain modifications induced by the appearance of a tumour as compare to the changes suffered after post-surgery. To that goal, we build networks from 8 different topological classes, considering several different parameter configurations. Then, we proceed to determine which one of the many networks being generated match best the network topology of the networks obtained from brain data describing two individuals, in which one has a small tumour and other with a large tumour, before and after surgery. Overall, we find that the Newman-

Watts small-world graph best reproduce the network topology from the patients with small and large tumour before surgery. Surgery radically alters the topology, once the best match for the network topology is the extended Barabási-Albert scale-free graph.

This paper is organised as follows: Section 2 describes the materials. Our results and discussions are explained in Section 3. Finally, our conclusions are described in Section 4.

2. Materials

2.1. Participants

Between May 2015 and October 2017, patients with a minimum age of 18 years old were recruited from Ghent University Hospital located in Belgium [4]. They had a supratentorial meningioma (WHO grade I or II) or glioma (WHO grade II or III) brain tumour and were scanned twice before and after the surgery. They considered 14 meningioma patients with mean age 60 years old and 11 glioma patients with mean age 47 years old [3]. After surgery, the data were collected on average 7.9 months post-operative.

In this work, we select two patients with a grade I meningioma and different size in the meninges [4]. One patient with a small tumour (size equal to 0.58 cm^3) is a female at an age of 49 years and another one is a female (60 years old) with a large tumour equal to 78.44 cm^3 . Based on the WHO grading system, grade I meningioma is the least malignant compared to grade II and III meningioma [5]. Malignancy is related to the speed of disease development, the extent of tumour penetration into healthy brain tissue, and the likelihood of progression or recurrence to higher degrees of malignancy [3]. The characteristics of the patients are described in Table 1.

Table 1: Patients features selected from Refs. [3, 4] for our study. The tumour histology is the meningioma I.

| Subjects | Sex | Age (year) | Handedness | Tumour lateralisation | Tumour location | Tumour size (cm^3) |
|-----------|--------|------------|--------------|-----------------------|-----------------|-------------------------------|
| Patient 1 | Female | 49 | Right-handed | Right | Frontal | 0.58 |
| Patient 2 | Female | 60 | Right-handed | Right | Parietal | 78.44 |

2.2. Structural connection matrices

For all participants, MRI scans were obtained using a Siemens 3T Magnetom Trio MRI scanner with a 32-channel head coil [4]. Aerts et al. [4] pre-processed T1-weighted anatomical MRI data using FreeSurfer (<http://surfer.nmr.mgh.harvard.edu>). They obtain a subject-specific parcellation of each subject’s brain into 68 cortical regions, containing 34 per hemisphere. They considered the default recon-all processing pipeline of FreeSurfer, including intensity normalisation, skull stripping, removal of non-brain tissue, brain mask generation, cortical reconstruction, segmentation of subcortical white matter. They also considered deep gray matter volumetric structures, cortical tessellation of the gray matter/white matter and gray matter/pial boundary, and construction of a probabilistic atlas based on cortical parcellation into 68 regions according to gyral and sulcal structure [5]. Furthermore, they constructed the structural connectomes based on the diffusion MRI (dMRI) data by means of a processing pipeline combining FSL (FMRIB’s Software Library) and MRtrix3. It was included correction for various artifacts (e.g., noise, motion, and eddy currents), registration of subjects’ high-resolution anatomical images to diffusion space, and segmentation of the anatomical images into gray matter, white matter and cerebrospinal fluid, as well as quantitative whole-brain probabilistic tractography. Then, aiming to build the structural connection matrices, each individual’s FreeSurfer parcellation scheme was transformed into diffusion MRI data and the number of estimated streamlines was calculated between each pair of brain regions. Finally, the SC matrices were thresholded and structural connections were normalised with the same constant scalar across participants as in the pre-operative analyses. Ensuring that all weights change between 0 and 1.

The experimentally measured fiber density is translated into a weighted matrix representing the intensities with which brain regions are interconnected. When the fiber density is not equal to 0, we transform the value into 1 in the adjacency matrix, otherwise into 0. In a structural connectivity matrix, we need to know if there is some connection between different brain regions. Our results remain robust if the real brain network is extracted with different threshold due to the fact that each element of a structural connectivity matrix, indicating 0 or 1.

Figure 1 illustrates how nodes in the brain connect to other nodes, where the colour code represents the weights. Figure 2 provides the names of each region represented as a node in the brain functional network. This representation transforms the weighted matrix into a symmetric adjacency matrix,

where 0 corresponds to no connection between the cortical areas (white regions) and 1 to connected areas (black regions). Figure 3 shows plots where the axes represent the regions as in Fig. 2, and black filled squares represent that any two regions are connected, for all the patients considered in this work, before and after surgery. The binarised connectivity (0 and 1) reduces the complexity and enhances the visual understanding [2]. Figures 3(a) and 3(b) represent the adjacency matrices for the patient 1 before and after surgery, respectively, while the adjacency matrices related to patient 2 are shown in Figs. 3(c) and 3(d). The regions from 0 to 33 are related to the left hemisphere and the regions from 34 to 67 are located at the right hemisphere.

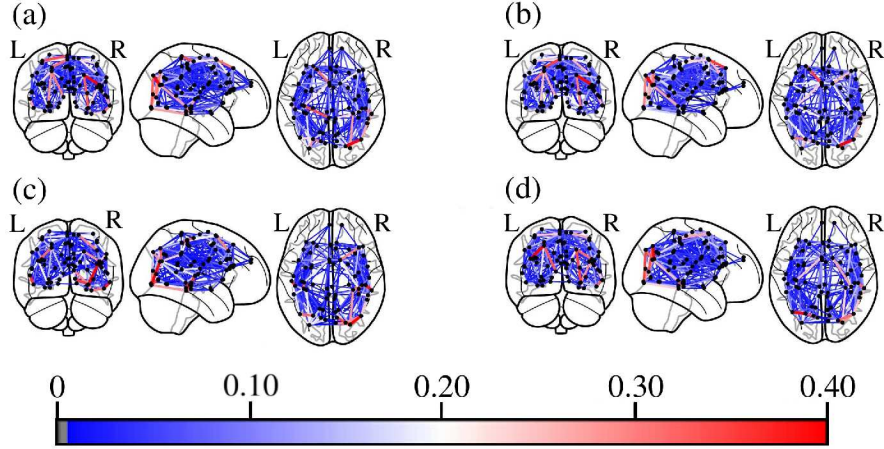


Figure 1: Connectome in the direction of the cuts: y (coronal), x (sagittal), and z (axial), respectively. For (a) patient 1 before surgery, (b) patient 1 after surgery, (c) patient 2 before surgery, and (d) patient 2 after surgery. The color bars indicate the amount of weights described as fiber density for each brain. Only 15% of the connections are considered, due to the fact that the graphs are very dense [3, 4]. We show the links which have an amount of connections greater than 85% of the maximum number of edges. L and R indicate the left and right hemispheres, respectively.

In Appendix, we include a Methods section making an introduction to Graph theory, the methods to generate different types of graphs, and the quantities considered to characterise the topology of the graph.

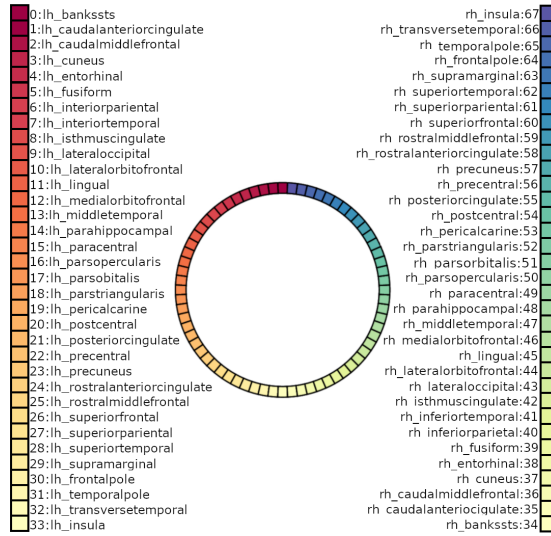


Figure 2: Circular graph of the 34 cortical regions for each hemisphere. Each region corresponds to a number from the range $[0,67]$, indicating the number of the cortical regions.

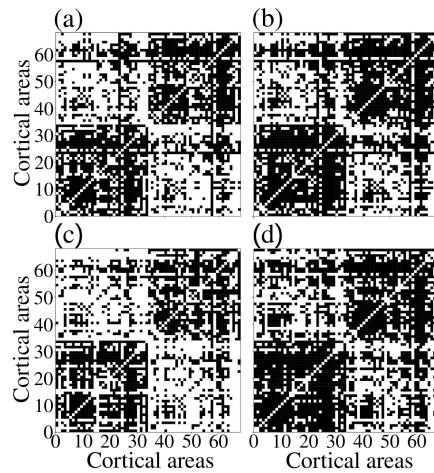


Figure 3: Adjacency matrices representing the structural connection of the patient's brains for (a) patient 1 before surgery, (b) patient 1 after surgery, (c) patient 2 before surgery, and (d) patient 2 after surgery. One (black colour) and zero (white colour) entries in the connection matrices mean connected and unconnected regions, respectively [3, 4].

3. Results and discussions

In our analysis, we consider 4 structural connectivity matrices obtained from two brain tumour patients before and after surgery according to Table 1. The structural connectivity matrix of the patient with small tumour before surgery consists of 68 nodes and 1200 edges, while the number of nodes equal to 68 and of edges equal to 1401 are for the same patient after surgery. The patient containing a large tumour has 68 nodes and 1036 edges before surgery, while after surgery the connection matrix of the same patient has 68 nodes and 1431 edges. We built 8 different networks with topologies similar to those detected in the human graphs obtained from the brain data. We consider 68 nodes and adjust the number of edges for each graph to be close to the individual graphs.

In order to design 8 classes of network topologies, we divide the brain data graphs into two groups, one for the patients with small and large tumour before surgery, as well as another for the patients with small and large tumour after surgery. The number of edges in each group is very similar.

3.1. *First group: before surgery brains*

We construct 8 different classes of graphs to compare each of them with the topology of the graphs from the brain data (before surgery brains) in terms of 9 topological features of networks, namely assortativity, average clustering, average shortest path length, density, global and local efficiency, modularity, radius, and transitivity. In Fig. 4, we build different Newman-Watts small-world (SW) graphs with the probabilities equal to 0.1, 0.3, 0.5, 0.7, and 0.9, representing as SW_1112, SW_1154, SW_1100, SW_1151 and SW_1168, respectively. The indexes correspond to the number of edges. We analyse the performance of them compared to the the networks of the two patients containing small tumour (Sb_1200) and large tumour (Lb_1036) before surgery.

To select the best small-world network among them, we calculate a percentage error (PE) between the features of each of them and those of the averaged over the two human subjects, including the two patients before surgery, due to the fact that these two subjects are very similar according to the metrics obtained for them in Fig. 4. The percent error is described as the difference between the measured value of that same topological feature calculated for the experimental brain data and the true value of a certain feature of the reproduced brain topology (using some network generator such

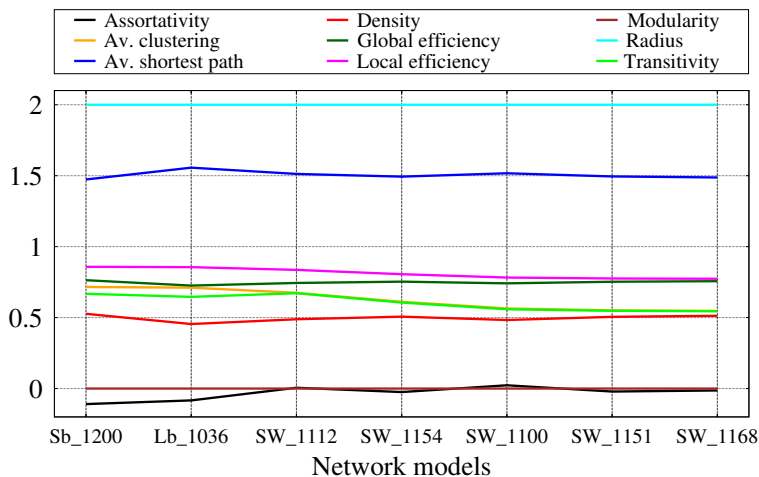


Figure 4: Representation of the 9 topological features for the 8 networks. Sb_1200 and Lb_1036 indicate the the patient with small tumour before surgery with 1200 edges and the patient with a large tumour before surgery with 1036 edges, respectively. SW_1112, SW_1154, SW_1100, SW_1151, and SW_1168 represent the small-world networks with the probabilities equal to 0.1, 0.3, 0.5, 0.7, and 0.9, respectively.

as small-world network), which is defined by

$$PE = \frac{|\text{Measured value} - \text{True value}|}{|\text{True value}|} 100\%, \quad (1)$$

A mean percentage error for each network topology is measured by the average of all the percent errors calculated for the features of that network. The average PE for all the small-world networks is illustrated in Fig. 5. The networks are SW_1112, SW_1154, SW_1100, SW_1151, SW_1168, and in Fig. 5 they are labeled as SW_0.1, SW_0.3, SW_0.5, SW_0.7, and SW_0.9, respectively. The results show that the mean percentage error obtained from the small-world network with 1112 edges and the probability equal to 0.1 is less than that of the remaining small-world networks. For $p < 0.1$, the Av. percentage error value slightly decreases.

After choosing the small-world with $p = 0.1$ (SW_0.1) as the best one among the other small-world networks, we construct more 7 networks: regular (Reg), random (R), Barabási-Albert scale-free (BA), extended Barabási-Albert scale-free (EBA), stochastic block community (Sto), random geometric spatial (RG), and Waxman random spatial (Wax) networks. They have the number of edges close to those of the data-based graph in this group.

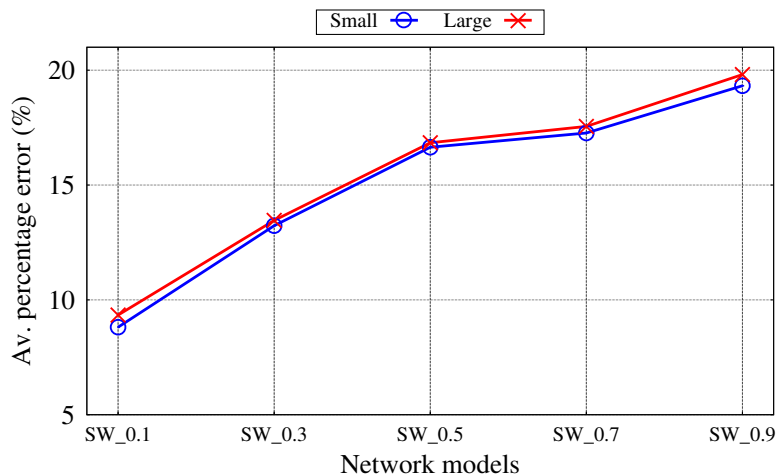


Figure 5: The average percentage error of the 5 small-world networks with different probabilities, describing as SW_0.1, SW_0.3, SW_0.5, SW_0.7 and SW_0.9, according to the percentage error calculated between the features of these 5 small-world networks and of the averaged over the two patients with small and large tumours before surgery. The x -axis labels describe the same Newman-Watts small-world with a different probability distribution.

The number of edges and the results obtained from the 9 structural features for each of them are displayed in Fig. 6, where the label means NETWORK #edges. By comparing the metrics, we find that the assortativity indicates a huge variation, radius is the same, and the remaining characteristics represent small alterations for all the graphs. For Reg_1156, the assortativity is undefined due to the fact that the denominator of the assortativity formula is zero [5].

We calculate the percentage error between the characteristics of each 8 graphs and of the averaged over the human subjects obtained from the brain data in this group. In Fig. 7, we verify that the best graph matching the two patients before surgery is the small-world network with the probability equal to 0.1. It exhibits an average PE less than 10%. We do not obtain an average percentage error for the regular network, due to the fact that the amount of assortativity feature calculated for this network topology is not defined.

3.2. Second group: after surgery brains

For the second group including the remaining two experimental brain networks after surgery, one patient with small tumour and another one with

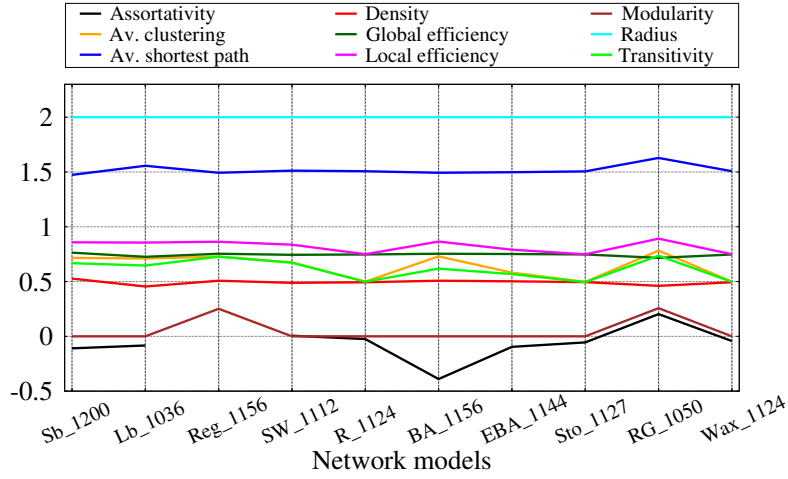


Figure 6: Representation of the 9 topological properties for the 11 graphs, describing the two experimental brains from the first group and the 8 graphs built according to the graph theory-based method. Reg, SW, R, BA, EBA, Sto, RG, and Wax correspond to the regular, small-world (with the probability equal to 0.1), random, Barabási-Albert scale-free, extended Barabási-Albert scale-free, stochastic block community, random geometric spatial, and Waxman random spatial networks, respectively. The number in the network name is the number of edges.

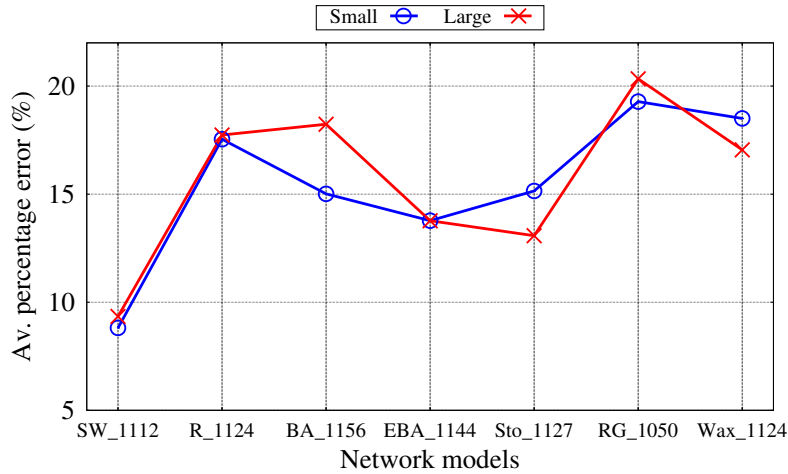


Figure 7: Representation of the average percentage error obtained for each network topology. The PE for each feature is calculated by comparing the averaged properties over the patients with small and large tumour before surgery with the generated networks based on graph theory. The x -axis labels indicate the different network topologies with variant features.

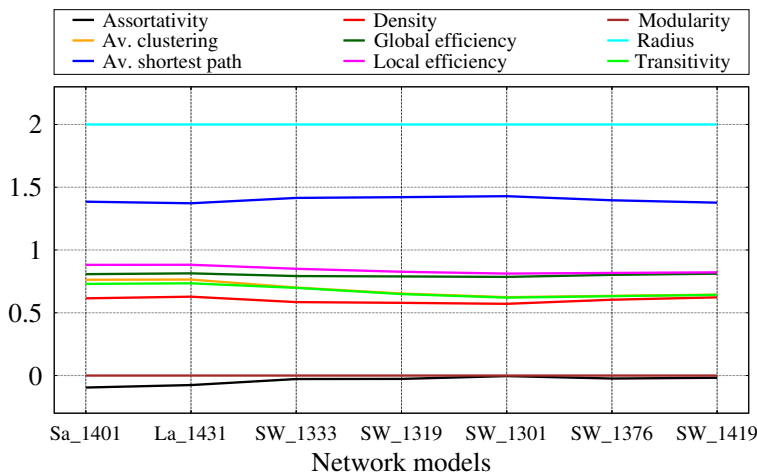


Figure 8: Representation of the 9 topological features for the 7 networks. Sa_1401 and La_1431 describe the patient with small and large tumour after surgery with 1401 and 1431 edges, respectively. SW_1333, SW_1319, SW_1301, SW_1376 and SW_1419 indicate the small-world networks with the probabilities equal to 0.1, 0.3, 0.5, 0.7 and 0.9, respectively.

large tumour, we compare them with the other 8 networks constructed based on graph theory. Both experimental network topologies are very similar to each other according to Fig. 8 and the metrics related to them and the generated networks do not significantly change. We compute the PE between the averaged features over the patients with small and large tumour after surgery and the properties of the 5 small-world networks. In Fig. 9, regarding the average PE calculated, we observe that the small-world graph with $p = 0.1$ has the mean percent error less than 10%, consequently, it is the best one to match with the two experimental networks as the first group.

In Fig. 10, we consider 8 different graphs, including the best small-world network selected, to compare them with the networks related to the patients in this group in terms of some structural measures. The results show that all the features, except the radius, change for each network. Furthermore, we calculate the PE between the characteristics of the averaged over the patients with small and large tumour after surgery and the other graphs shown in Fig. 10. From Fig. 11, we conclude that the best network adapted with the brain data graphs with the mean percent error less than 5% is the extended Barabási-Albert network with 1386 edges. Like the first group, we do not calculate a mean PE for the regular network, due to the fact that the amount of assortativity feature measured for this topology is not defined.

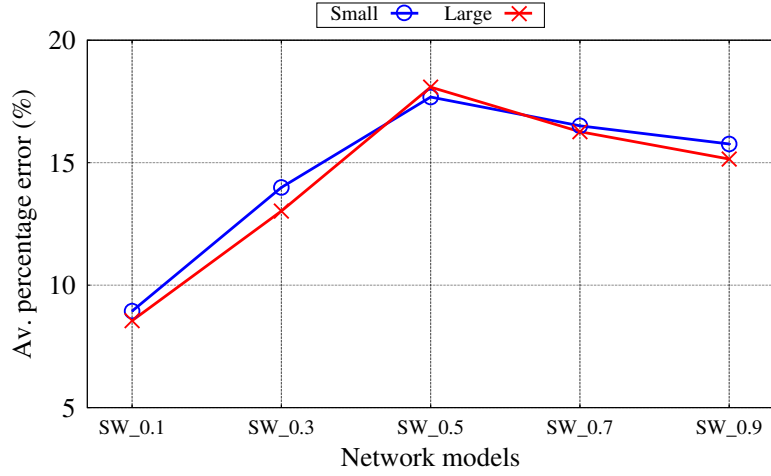


Figure 9: The average percentage error measured according to the percent error calculated between the features of the averaged over the two patients with small and large tumour after surgery and of the 5 small-world networks with the probabilities equal to 0.1, 0.3, 0.5, 0.7, and 0.9, representing as SW_0.1, SW_0.3, SW_0.5, SW_0.7 and SW_0.9, respectively. The x -axis labels describe the same Newman-Watts small-world with a different probability distribution.

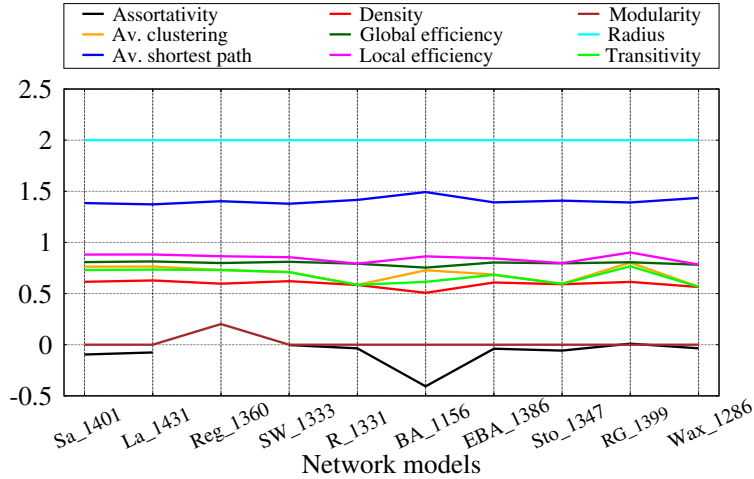


Figure 10: Illustration of the 9 topological properties for the 10 graphs, including the two experimental brains after surgery and the 8 graphs built according to the graph theory-based methods. Reg, SW, R, BA, EBA, Sto, RG, and Wax indicate regular, small-world (with the probability equal to 0.1), random, Barabási-Albert scale-free, extended Barabási-Albert scale-free, stochastic block community, random geometric spatial and Waxman random spatial networks, respectively. The number in each network name corresponds to the number of edges.

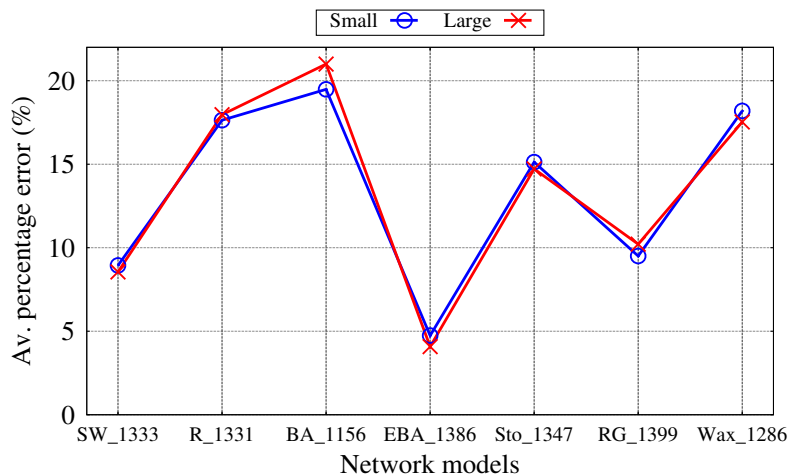


Figure 11: Representation of the average PE obtained for each network topology. The PE for each feature is calculated by comparing the averaged properties over the patients with small and large tumour after surgery with the generated networks based on graph theory.

In our numerical simulations, we do not calculate a percentage error for the modularity feature, due to the fact that it is zero in the networks obtained from the brain data (two patients).

4. Conclusions

We consider adjacency matrices representing 68 different cortical regions of the structural connectivity of the brain. The matrices are related to different brains, two for patients with small and large tumour before and after surgery. We then generate several networks with 8 different network topologies (small-world, scale-free, etc) and different parameter configurations. We compare the graphs from the brain data with these generated networks for several network features considered (radius, modularity, etc) and calculate the average percentage error (PE) quantifying how similar the generated graphs are from the graphs representing the structural connectivity of patients with tumour before and after surgery.

Regarding network topologies properties, our results show no significant differences in global efficiency and modularity in the brain tumour patients before and after surgery which corroborate the previous studies [3, 4]. We, however, find much significantly greater connection density and less shortest path length in the patients after surgery than in the patients before surgery.

The enhanced density in the tumour patients after surgery suggests that surgery may induce reorganisation in the structural network topology, so that we show that surgery causes significantly topological alterations in the patients with small and large tumour. Also, the remaining characteristics represent no significant alterations between the brain data graphs before and after surgery.

In this work, our focus is on the best fit for the groups. We calculate 9 topological properties to compute the average percentage error for each network. By means of the average percentage error, we obtain the relative error between generated networks and matrices selected from cortical regions of the brain structural connectivity. For the brains with small and large tumour before surgery, we verify that the best network topology with the average percentage error less than 10% is the Newman-Watts small-world with the probability equal to 0.1. For this probability value, the Newman-Watts and Watts-Strogatz networks have the same small-world properties, which is high transitivity or clustering with a low average path lengths. For the two individuals after surgery, one with small tumour and another with large tumour, the best graph with the average percent error less than 5% is the extended Barabási-Albert scale-free network topology.

Our main conclusion is that the network topologies based on small-world and scale-free graphs can be useful to respectively describe a brain network topology considered for the brain tumour patients before surgery and brain tumour patients after surgery, respectively. The selected patients were diagnosed with a meningioma tumour. It is a type of benign brain tumour that grows slowly and does not spread to the whole brain or central nervous system. It has been shown that disturbances in network topology could be seen even for individuals with meningioma tumours [5]. In our outcomes based on the 9 topological features, we observe a small change between the brain networks related to the patients before surgery. We identify the best network topology matching with the brain networks after surgery without considering the tumour location.

Knowing that a scale-free network can be transformed into a small-world one by the addition of a small number of random “weak” links (many long-range) to the scale-free network, makes us to wonder whether the surgery, or brain adaptations necessary post-surgery, have not effectively reduced the random weak long-range linkage of the brain, giving to it the scale-free structure observed in this work. We hope further work can help better elucidate this hypothesis.

In our analyses, we choose two adjacency matrices from 14 meningioma patients. We select the patients according to the tumour size, the smallest and largest tumours. In our study, we use two patients with different size of tumour. Neuronal imaging data normally contains large extent of noise and there is variance among subjects. Due to these facts, it is impossible to obtain general conclusions and more analysis is required. In future works, we plan to select more patients to investigate how our results change when the same study is made.

We believe that there are possible applications of our findings in further precision treatment of tumours. Similar application in epilepsy surgery was reported by Wang et al. [5]. They reported strategies of surgical seizure control to identify and remove fewer anatomical connections that are responsible for spread of seizures.

Acknowledgments

This study was possible by partial financial support from the following agencies: Fundação Araucária, Brazilian National Council for Scientific and Technological Development (CNPq), and Coordination for the Improvement of Higher Education Personnel (CAPES). São Paulo Research Foundation (FAPESP 2018/03211-6, 2022/13761-9). We thank 105 Group Science (www.105groupscience.com).

Appendix A. Methods

Appendix A.1. Graph theory analysis

A graph consists of a finite set of nodes (or vertices) connected by links called edges or arcs [5]. In graph theory, the $N \times N$ adjacency matrix with zero and non-zero elements, also known as connectivity matrix, indicates the absence and presence of a relationship between the nodes of a network, respectively. Using a graph theory-based method, it is possible to obtain a topological analysis of the human brain network using different metrics from its structural connection matrix, due to the fact that the brain can be considered as a large and complex network. In neuroscience studies, the main capability of graph theory is usually revealed after constructing a brain network [5]. Then, there are many different graph generators, such as regular, small-world, random (without structure), scale-free (hub structure), community structure, and spatially embedded graphs to describe the topology of the brain networks.

Appendix A.1.1. Small-world and regular networks

Watts and Strogatz [2] introduced small-world networks. A small-world exhibits a high degree of clustering as in the regular networks, where all nodes have the same number of neighbours. It has a small average distance between the nodes as in the random networks and has intermediate connectivity attributes [5]. In the small-world networks introduced by Watts and Strogatz, non-local links are inserted by randomly rewiring some local connections into non-local ones [2], while randomly selected shortcuts are added in a regular lattice by Newman and Watts [5]. A schematic representation related to the regular and Newman–Watts small-world graphs are shown in Figs. 12(a) and 12(b), respectively.

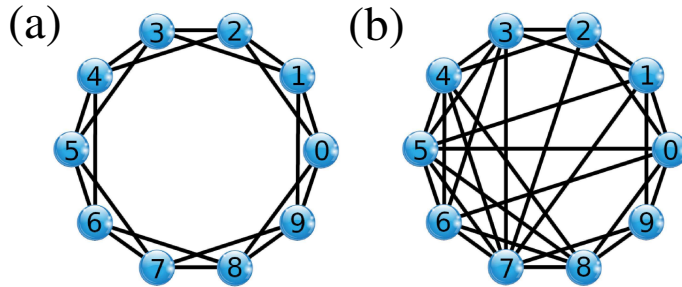


Figure A.12: Structural representation of (a) a regular graph for 10 nodes that are connected to their 4 nearest neighbours and (b) a Newman-Watts small-world graph for $N = 10$.

Appendix A.1.2. Random network

In a random network, the nodes are randomly connected by means of a pre-determined connection probability [5]. The random graph has low clustering and short path length. In 1959, Erdős and Rényi [6] introduced a random graph called Erdős-Rényi model or binomial graph. Figure 13 displays a graph representation of a random network.

Appendix A.1.3. Scale-free network

A scale-free network is a network in which degree distribution, describing the number of links adjacent to a node, follows a power law, at least asymptotically [6]. It means that after the removal of randomly selected nodes, the graph stays more connected than a random network and has short average path lengths [6].

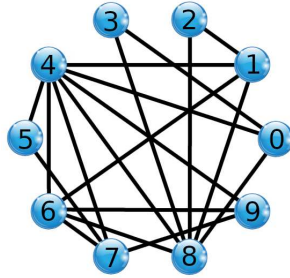


Figure A.13: Schematic representation of an Erdős-Rényi random network for $N = 10$ nodes and $p = 0.4$.

In a scale-free graph, there are growth and preferential attachments. In this regard, the network grows by continuously adding new nodes at every time step and, regarding preferential attachment, the probability of linking to a node depends on the node's degree [6]. Barabási and Albert [6] proposed an algorithm for generating random scale-free networks using a growth and preferential attachment mechanism. Figures 14(a) and 14(b) show a representation of Barabási-Albert and extended Barabási-Albert networks, respectively.

The Barabási-Albert model is an undirected scale-free network with a hub structure (heavy-tailed degree distribution). The graph grows by connecting new nodes preferentially to existing high-degree nodes. This way, it is created a rich club of centralised hubs that connect otherwise distant areas of the graph. The extended Barabási-Albert graph is a type of undirected scale-free graphs. It is a random graph built using preferential attachment, which permits new nodes, new edges or rewiring edges. Considering p as the probability value for adding an edge between existing nodes and q as the probability value of rewiring of existing edges ($p + q < 1$), the model behaves just like the Barabási-Albert model when $p = q = 0$.

Appendix A.1.4. Community structure network

A community structure network has nodes that can be easily classified into (potentially overlapping) sets of nodes, such that each set of nodes is densely linked internally [6]. In 1983, Holland et al. [6] introduced a mathematical formulation for a stochastic block model, as an useful benchmark to recover community structure in graph data in the field of social network. Afterward, researchers have generated networks with a defined community structure using stochastic block model [6]. In Fig. 15, a stochastic block

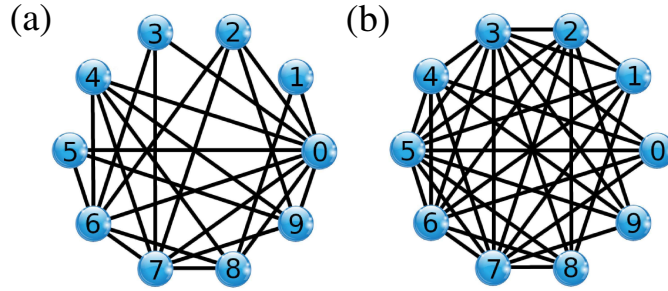


Figure A.14: Schematic representation of (a) a Barabási-Albert graph for $N = 10$ and (b) an extended Barabási-Albert graph.

model has been illustrated.

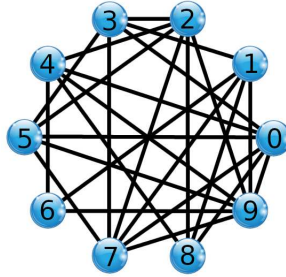


Figure A.15: Schematic representation of a generative stochastic block model for 2 communities with the size 5 ($s = 5$) and the probability equal to 0.5 ($p = 0.5$). The community 1 contains the nodes 0, 1, 2, 3, and 4. The community 2 starts from the node 5 to 9.

Appendix A.1.5. Spatially embedded network

A spatial (geometric) network consists of spatial components that limit the network structure and provide a framework for network models containing spatial elements [6]. In the graph, nodes are embedded in the space and a metric is considered to dictate the conditions for links between nodes [6]. Most models of this graph assume Euclidean distance in 2 or 3-dimensions for the probability of connection [7]. In 2011, Marc Barthélemy [6] provided a general overview of spatial network models and of the most important theoretical evidence used for the spatially embedded networks. An undirected

and without self-loops random geometric graph, as well as a Waxman random graph have been exhibited in Figs. 16(a) and 16(b), respectively.

In the random geometric graph, the nodes are randomly distributed in the same metric space. Two nodes are connected by an edge when their distance is smaller than a certain range. In the Waxman random model, as the spatial generalisation of Erdős–Rényi random networks, the nodes are uniformly distributed in a rectangular domain. Each pair of nodes is connected by an edge with a probability that depends on a function of the distance between them. The function is exponential, as proposed by Waxman, and plays an important role in determining the structure of a Waxman graph.

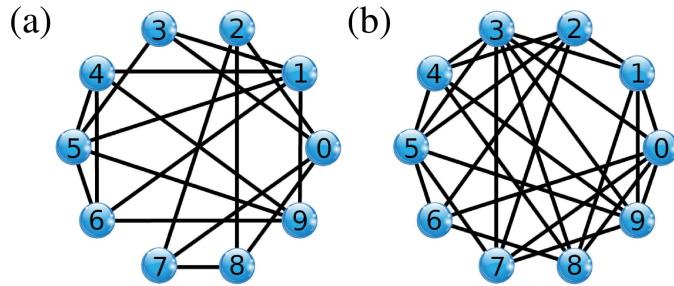


Figure A.16: Schematic representation of (a) a random geometric graph for $N = 10$ and $r = 0.5$ and (b) a Waxman random graph for $N = 10$ and $p = 0.4$.

Appendix A.2. Topological characteristics of graphs

To analyse the structural patterns of the networks, we compute some measures related to the integration and segregation, such as assortativity, average clustering, average shortest path length, density, global and local efficiency, modularity, radius, and transitivity. The integration feature is associated with the ability of the network to transmit information through its nodes, while the segregation property is related to the presence of clusters or modules in a graph [7]. In other words, the segregation and integration describe the network characteristics [2].

Appendix A.2.1. Assortativity

Assortativity (A) refers to the tendency of the nodes to link with other similar nodes over dissimilar nodes, while in disassortativity, the nodes tend to connect to dissimilar nodes over similar nodes. The assortativity measures

the similarity of connections with respect to the node degree [7]. A is defined in the interval $[-1, 1]$. The network is perfect assortative when $A = 1$, not assortative when $A = 0$, and completely disassortative when $A = -1$. A positive assortativity coefficient indicates a correlation between nodes of similar degrees, while a negative one shows a correlation between nodes of different degrees. In fact, the degree assortativity coefficient is the same as the Pearson correlation coefficient of degree between pairs of connected nodes [7].

Appendix A.2.2. Average clustering coefficient

A clustering coefficient measures the degree and indicates the tendency of the nodes in a graph to cluster together [7]. For a network, the average clustering coefficient can be calculated using the average of clustering coefficients of all the nodes. When the graph is more complete, the connections are dense and the average clustering coefficient is high. It is a sign of triadic closure due to the fact that the more complete the graph is, the more triangles usually arise [7]. The average clustering coefficient (ACC) provides a measure of modularity of the network. When the average clustering coefficient is 1, the neighbourhood of the node is fully connected. For ACC close to 0, there are almost no connections in the neighbourhood.

Appendix A.2.3. Average shortest path length

The average shortest path length ($ASPL$), also known as average path length, is described as the average number of edges along the shortest paths for all possible pairs of nodes in the graph [7]. It measures the efficiency of information or mass transport on a graph. From one node to another in the network, the average path length is an average over the shortest distance between two nodes.

Appendix A.2.4. Density

The density (D) of a graph describes the ratio of the number of edges with respect to the maximum possible edges [7]. It provides a relationship between a density of graph and edge connectivity. The graph is dense when the quantity of edges is close to the maximal number of edges and each pair of vertices has one edge. When the density is equal to 0, the graph is without edges. For a density equal to 1, the graph is completely connected.

Appendix A.2.5. Global efficiency

Efficiency of a pair of nodes in a graph is the multiplicative inverse of the shortest path distance between the nodes [7]. The average global efficiency (*AGE*) of a graph is the average efficiency of all pairs of nodes or the graph. $0 \leq AGE \leq 1$ is a normalised measure where its maximum value is reached when a graph is complete. It returns 0 if there is no path between the nodes.

Appendix A.2.6. Local efficiency

Efficiency of a graph, also known communication efficiency, measures the efficiency of the information exchange [7]. In the network, if the distance between two nodes is greater, their communication is less efficient. This measurement can deal with the disconnected graphs, non-scattered graphs or both [7]. The local efficiency (*LE*) of a node in the graph is the average global efficiency of the subgraph induced by the node's neighbours. This measurement changes in the interval [0,1]. If there is no path between nodes in the graph, the average local efficiency of the graph returns 0.

Appendix A.2.7. Modularity

Graphs can be separated into two or more modules. When a graph is grouped into two modules, one module has one node and another one consists of all the remaining nodes. Then, the modularity (*M*) refers to the degree in which a network is organised into a modular structure or community [8]. Modules are subgraphs that contain sets of nodes which are more strongly linked to each other than to the rest of the graph [8]. *M* can be positive or negative, the positive values indicate the possible existence of community structure.

Appendix A.2.8. Radius

The eccentricity of a node in a graph is the maximum distance from it to all other nodes [8]. The radius (*R*) of a graph is the minimum distance among all the maximum distances between a node and all other nodes [8].

The radius exists in a graph only if the graph has the diameter as the maximum eccentricity. This metric is considered for distance measurement purposes, which is described as

$$R = \text{Min } d(n_i, n_{i \neq j}), \quad (\text{A.1})$$

where $d(n_i, n_{i \neq j})$ is the distance between the node i and the remaining nodes in the graph. The curve is a circle if the eccentricity is equal to zero, a

parabola if equal to one, an ellipse if less than one, and a hyperbole if greater than one. The radius of a graph is the minimum graph eccentricity of some vertex. A disconnected graph has an infinite radius.

Appendix A.2.9. Transitivity

The transitivity (T) is described as the fraction of all possible triangles in a graph. The possible triangles are determined by the number of triads, describing two edges with a shared node [8]. This measurement is also known as the amount of clustering between a node and its neighbours. When $T = 1$, the network consists of all possible edges.

References

- [1] G.M. Cooper, The development and causes of cancer, The cell: a molecular approach 2nd edition Sunderland (MA), Sinauer Associates (2000).
- [2] M. Tubiana, Tumor cell proliferation kinetics and tumor growth rate, Acta Oncol 28 (1989) 113-21.
- [3] H. Aerts, M. Schirner, T. Dhollander, B. Jeurissen, E. Achten, D.V. Roost, P. Ritter, D. Marinazzo, Modeling brain dynamics after tumor resection using The Virtual Brain, NeuroImage 213 (2020) 116738.
- [4] N. Gordillo, E. Montseny, P. Sobrevilla, State of the art survey on MRI brain tumor segmentation, Magn Reson Imaging 31 (2013) 1426-1438.
- [5] S.M. LaConte, Decoding fMRI brain state in real-time, NeuroImage 56 (2011) 440-454.
- [6] H.T. Chugani, M.E. Phelps, J.C. Mazziotta, Positron emission tomography study of human brain functional development, Ann Neurol 22 (1987) 487-497.
- [7] S. Ogawa, T.M. Lee, A.R. Kay, D.W. Tank, Brain magnetic resonance imaging with contrast dependent on blood oxygenation, Proc Natl Acad Sci USA 87 (1990) 9868-9872.
- [8] G. Pfurtscheller, F.H. Lopes, Event-related EEG/MEG synchronization and desynchronization: basic principles, Clin Neurophysiol 110 (1999) 1842-1857.

- [9] C. Golgi, On the Structure of the Gray Matter of the Brain, *Gazzetta Medica Italiana. Lombardia* 33 (1873) 244-246.
- [10] S.R. y Cajal, Estructura de los centros nerviosos de las aves, *Rev Trim Hist Norm Pat* (1888).
- [11] G.M. Shepherd, *Foundations of the neuron doctrine*, Oxford University Press (2015).
- [12] J. Hsieh, *Computed tomography: principles, design, artifacts, and recent advances*, SPIE Bellingham, WA (2009).
- [13] C. Pierpaoli, P. Jezzard, P.J. Basser, A. Barnett, G. Di Chiro, Diffusion tensor MR imaging of the human brain, *Radiology* 201 (1996) 637-648.
- [14] P.J. Basser, S. Pajevic, C. Pierpaoli, J. Duda, A. Aldroubi, In vivo fiber tractography using DT-MRI data, *Magn Reson Med* 44 (2000) 625-632.
- [15] C.C. Hilgetag, G.A. Burns, M.A. O'Neil, J.W. Scannell, M.P. Young, Anatomical connectivity defines the organization of clusters of cortical areas in the macaque monkey and the cat, *Philos Trans R Soc Lond B* 355 (2000) 91-10.
- [16] S.L. Bressler, Large-scale cortical networks and cognition, *Brain Res Rev* 20 (1995) 288-304.
- [17] J.W. Essam, M.E. Fisher, Some basic definitions in graph theory, *Rev Mod Phys* 42 (1970) 271-288.
- [18] O. Sporns, G. Tononi, R. Kötter, The human connectome: a structural description of the human brain, *PLoS Comput Biol* 1 (2005) e42.
- [19] O. Sporns, The human connectome: origins and challenges, *Neuroimage* 80 (2013) 53-61.
- [20] F.V. Farahani, W. Karwowski, N.R. Lighthall, Application of Graph Theory for Identifying Connectivity Patterns in Human Brain Networks: A Systematic Review, *Frontiers in Neuroscience* 13 (2019) 585.
- [21] M. Zain, X. Sun, S. Wandelt, Studying the Topology of Transportation Systems through Complex Networks: Handle with Care, *Journal of Advanced Transportation* 3156137 (2018) 17.

- [22] M.J. Krawczyk, L. Muchnik, A. Mańka-Krasoń, K. Kulakowski, Line graphs as social networks, *Physica A* 390 (2011) 2611-2618.
- [23] G. Hernández, E. Zamora, H. Sossa, G. Téllez, F. Furlán, Hybrid neural networks for big data classification, *Neurocomputing* 390 (2020) 327-340.
- [24] D.J. Watts, S.H. Strogatz, Collective dynamics of “small-world” networks, *Nature* 393 (1998) 440-442.
- [25] F. Schweitzer, G. Fagiolo, D. Sornette, F. Vega-Redondo, A. Vespignani, A., D.R. White, Economic networks: the new challenges, *Science* 325 (2009) 422-425.
- [26] L. Euler, *Solutio problematis ad geometriam situs pertinentis*, *Comment Acad Sci Imp Petropolitanae* 8 (1736) 128-140.
- [27] E. Bullmore, O. Sporns, The economy of brain network organization, *Nat Rev Neurosci* 13 (2012) 336-349.
- [28] N. Kriegeskorte, P.K. Douglas, Cognitive computational neuroscience, *Nat Neurosci* 21 (2018) 1148-1160.
- [29] M. Newman, *Networks*. Oxford University Press, 2018.
- [30] X. Liao, A.V. Vasilakos, Y. He, Small-world human brain networks: perspectives and challenges, *Neurosci Biobehav Rev* 77 (2017) 286-300.
- [31] E.T. Bullmore, Simple models of human brain functional networks, *Proc Natl Acad Sci USA* 109 (2012) 5868-5873.
- [32] Y. Chen, S. Wang, C.C. Hilgetag, C. Zhou, Trade-off between multiple constraints enables simultaneous formation of modules and hubs in neural systems, *PLoS Comput Biol* 9 (2013) e1002937.
- [33] D.S. Bassett, N.F. Wymbs, M.A. Porter, P.J. Mucha, J.M. Carlson, S.T. Grafton, Dynamic reconfiguration of human brain networks during learning, *Proc Natl Acad Sci USA* 108 (2011) 7641-7646.
- [34] M. Cao, H. Huang, Y. Peng, Q. Dong, Y. He, Toward developmental connectomics of the human brain, *Front Neuroanat* 10 (2016) 25.

- [35] M. Jalili, Graph theoretical analysis of Alzheimer’s disease: discrimination of AD patients from healthy subjects, *Inf Sci* 384 (2017) 145-156.
- [36] S.N. Miri Ashtiani, M.R. Daliri, H. Behnam, G.A. Hossein-Zadeh, M. Mehrpour, M.R. Motamed, F. Fadaie, Altered topological properties of brain networks in the early MS patients revealed by cognitive task-related fMRI and graph theory, *Biomed. Signal Process Control* 40 (2018) 385-395.
- [37] P.R. Protachevicz, F.S. Borges, E.L. Lameu, P. Ji, K.C. Iarosz, A.H. Kihara, I.L. Caldas, J.D. Szezech Jr., M.S. Baptista, E.E.N. Macau, C.G. Antonopoulos, A.M. Batista, J. Kurths, Bistable Firing Pattern in a Neural Network Model, *Front Comput Neurosci* 13 (2019) 13-19.
- [38] Y. He, Z. Chen, A. Evans, Structural insights into Aberrant Topological patterns of large-scale cortical networks in Alzheimer’s Disease, *J Neurosci* 28 (2008) 4756-4766.
- [39] E. Courchesne, K. Pierce, Why the frontal cortex in autism might be talking only to itself: local over-connectivity but long-distance disconnection, *Curr Opin Neurobiol* 15 (2005) 225-230.
- [40] Y. He, A. Dagher, Z. Chen, A. Charil, A. Zijdenbos, K. Worsley, A. Evans, Impaired small-world efficiency in structural cortical networks in multiple sclerosis associated with white matter lesion load, *Brain* 132 (2009) 3366-3379.
- [41] Y. Wang, C. Zuo, Q. Xu, S. Liao, M. Kanji, D. Wang, Altered resting functional network topology assessed using graph theory in youth with attention-deficit/hyperactivity disorder, *Prog Neuro-Psychoph Biol Psychiatry* 98 (2020) 109796.
- [42] A. Calderone, M. Formenti, F. Aprea, M. Papa, L. Alberghina, A.M. Colangelo, P. Bertolazzi, Comparing Alzheimer’s and Parkinson’s diseases networks using graph communities structure, *BMC Systems Biology* 10 (2016) 10-25.
- [43] D. Zhi, V.D. Calhoun, L. Lv, X. Ma, Q. Ke, Z. Fu, Aberrant dynamic functional network connectivity and graph properties in major depressive disorder, *Front Psychiatry* 9 (2018) 339.

- [44] Z. Li, R. Chen, M. Guan, E. Wang, T. Qian, C. Zhao, Disrupted brain network topology in chronic insomnia disorder: a resting-state fMRI study, *NeuroImage Clin.* 18 (2018) 178-185.
- [45] T. Xu, K.R. Cullen, B. Mueller, M.W. Schreiner, K.O. Lim, S.C. Schulz, K.K. Parhi, Network analysis of functional brain connectivity in borderline personality disorder using resting-state fMRI, *NeuroImage: Clin.* 11 (2016) 302-315.
- [46] R.F. Algunaid, A.H. Algumaei, M.A. Rushdi, I.A. Yassine, Schizophrenic patient identification using graph-theoretic features of resting-state fMRI data, *Biomed Signal Process Control* 43 (2018) 289-299.
- [47] C.C. Armstrong, T.D. Moody, J.D. Feusner, J.T. McCracken, S. Chang, J.G. Levitt, J.C. Piacentini, J. O'Neill, Graph-theoretical analysis of resting-state fMRI in pediatric obsessive-compulsive disorder, *J Affect Disord* 193 (2016) 175-184.
- [48] Z. Yu, L. Tao, Z. Qian, J. Wu, H. Liu, Y. Yu, J. Song, S. Wang, J. Sun, Altered brain anatomical networks and disturbed connection density in brain tumor patients revealed by diffusion tensor tractography, *Int J Comput Assist Radiol Surg* 11 (2016) 2007–2019.
- [49] H. Aerts, M. Schirner, B. Jeurissen, D.V. Roost, E. Achten, P. Ritter, D. Marinazzo, Modeling brain dynamics in brain tumor patients using the virtual brain, *eNeuro* 5 (2018) 1-15.
- [50] B. Fischl, A. van der Kouwe, C. Destrieux, E. Halgren, F. Ségonne, D.H. Salat, E. Busa, L.J. Seidman, J. Goldstein, D. Kennedy, V. Caviness, N. Makris, B. Rosen, A.M. Dale, Automatically parcellating the human cerebral cortex, *Cereb Cortex* 14 (2004) 11-22.
- [51] D.N. Louis, H. Ohgaki, O.D. Wiestler, W.K. Cavenee, P.C. Burger, A. Jouvett, B.W. Scheithauer, P. Kleihues, The 2007 WHO classification of tumours of the central nervous system, *Acta Neuropathol* 114 (2007) 97-109.
- [52] A. Arcagni, R. Grassi, S. Stefani, A. Torriero, Higher order assortativity in complex networks, *European Journal of Operational Research* 262 (2017) 708-719.

- [53] J. Derks, J.C. Reijneveld, L. Douw, Neural network alterations underlie cognitive deficits in brain tumor patients, *Curr Opin Oncol* 26 (2014) 627-633.
- [54] C. Wang, S. Chen, L. Huang, L. Yu, Prediction and control of local seizure spread: Random walk with restart on heterogeneous brain networks, *Phys Rev E* 105 (2022) 064412.
- [55] R. Gould, *Graph theory*, Courier Corporation, New York (2012).
- [56] M.P. Van Den Heuvel, C.J. Stam, M. Boersma, H.E. Hulshoff Pol, Small-world and scale-free organization of voxel-based resting-state functional connectivity in the human brain, *Neuroimage* 43 (2008) 528-539.
- [57] D.J. Watts, *Small Worlds: The Dynamics of Networks Between Order and Randomness*, Princeton University Press (1999).
- [58] M.E.J. Newman, D. J. Watts, Renormalization group analysis of the small-world network model, *Phys Lett A* 263 (1999) 341.
- [59] N. Gilbert, Random Graphs, *Ann Math Stat* 30 (1959) 1141.
- [60] P. Erdős, A. Rényi, On Random Graphs, *Publ Math* 6 (1959) 290.
- [61] A. Pachon, L. Sacerdote, S. Yang, Scale-free behavior of networks with the copresence of preferential and uniform attachment rules, *Physica D* 371 (2018) 1-12.
- [62] O. Sporns, D.R. Chialvo, M. Kaiser, C.C. Hilgetag, Organization, development and function of complex brain networks, *Trends Cogn Sci* 8 (2004) 418-425.
- [63] P. Krapivsky, D. Krioukov, Dmitri, Scale-free networks as preasymptotic regimes of superlinear preferential attachment, *Phys Rev E* 78 (2008) 026114.
- [64] A.L. Barabási, R. Albert, Emergence of scaling in random networks, *Science* 286 (1999) 509-512.
- [65] M. Girvan, M.E.J. Newman, Community structure in social and biological networks, *Proc Natl Acad Sci USA*. 99 (2002) 7821-7826.

- [66] P.W. Holland, K.B. Laskey, S. Leinhardt, Stochastic blockmodels: First steps, *Soc Netw* 5 (1983) 109-137.
- [67] C. Icher, A.Z. Jacobs, A. Clauset, Learning latent block structure in weighted networks, *J Complex Netw* 3 (2015) 221-248.
- [68] M. Penrose, *Random Geometric Graphs*, Oxford Studies in Probability 5 (2003).
- [69] M. Barthelemy, Spatial Networks, *Phys Rep* 499 (2011) 1-101.
- [70] C. Parkinson, S. Liu, T.A. Wheatley, Common cortical metric for spatial, temporal, and social distance, *J. Neurosci.* 34 (2014) 1979-1987.
- [71] M. Rubinov, O. Sporns, Complex network measures of brain connectivity: uses and interpretations, *Neuroimage* 52 (2010) 1059-1069.
- [72] M.E.J. Newman, Mixing patterns in networks, *Phys Rev E* 67 (2003) 026126.
- [73] J.G. Foster, D.V. Foster, P. Grassberger, M. Paczuski, Edge direction and the structure of networks, *Proc Natl Acad Sci USA* 107 (2010) 10815-10820.
- [74] J. Sarämki, M. Kivelä, J.P. Onnela, K. Kaski, and J. Kertész, Generalizations of the clustering coefficient to weighted complex networks, *Phys Rev E* 75 (2007) 027105.
- [75] G. Costantini, M. Perugini, Generalization of Clustering Coefficients to Signed Correlation Networks, *PloS One* 9 (2014) e88669.
- [76] T. Opsahl, F. Agneessens, J. Skvoretz, Node centrality in weighted networks: Generalizing degree and shortest paths, *Soc Netw* 32 (2010) 245-251.
- [77] R. Diestel, Reinhard, *Graph Theory*, Graduate Texts in Mathematics, Springer-Verlag (2005).
- [78] V. Latora, M. Marchiori, Efficient behavior of small-world networks, *Phys Rev Lett* 87 (2001) 198701.

- [79] D.S. Bassett, E. Bullmore, Small-world brain networks, *Neuroscientist* 12 (2006) 512-523.
- [80] M.E.J. Newman, Modularity and community structure in networks, *Proc Natl Acad Sci USA* 103 (2006) 8577-8582.
- [81] M.E.J. Newman, *Networks: An Introduction*, Oxford University Press (2011) 224.
- [82] J. Bouttier, P. Di Francesco, E. Guitter, Geodesic distance in planar graphs, *Nucl Phys B* 663 (2003) 535-567.
- [83] D.B. West, *Introduction to Graph Theory*, 2nd ed. Englewood Cliffs, NJ: Prentice-Hall (2000).
- [84] T. Opsahl, P. Panzarasa, Clustering in weighted networks, *Soc. Netw.* 31 (2009) 155-163.